

Fabrication of clickable bamboo-sourced cellulose nanofibrils for diverse surface modifications: Hydrophobicity and fluorescence functionalities

Juan Long, Zhiqiang Li, Tuhua Zhong*

International Centre for Bamboo and Rattan, Beijing 100102, China

Key Laboratory of NFGA/Beijing for Bamboo & Rattan Science and Technology, National Forestry and Grassland Administration, Beijing 100102, China

ARTICLE INFO

Keywords:

Bamboo
Nanofibrillation
Surface modification
Click chemistry
Functionality

ABSTRACT

Surface functionalization of cellulose nanofibrils (CNF) is crucial for expanding their practical application. However, most functionalization processes are complicated and laborious. Herein, this work presents a facile surface engineering strategy to create a range of functionalized CNF via thiol-ene click reaction. Initially, clickable CNF was produced by grafting a compound with both carboxylate- and norbornene groups onto bamboo cellulose via norbornene-dicarboxylic anhydride esterification followed by homogenization. The introduction of negatively charged carboxylates facilitated nanofibrillation, resulting in CNF with a diameter of 3 nm and an aspect ratio of up to 600. The introduction of norbornenes enabled diverse functionalization of CNF through click reaction. Subsequently, hexadecanethiol successfully clicked with norbornene-grafting CNF, enhancing its hydrophobicity and dispersion in organic solvents. 7-mercapto-4-methyl coumarin was also able to click with norbornene-grafting CNF, yielding fluorescence-labeled CNF while maintaining excellent aqueous dispersibility. The fluorescence-labeled CNF was demonstrated to be utilized as an eco-friendly sensor for the detection of Fe³⁺ ions. Additionally, it could be converted into fluorescent films or intelligent inks suitable for anti-counterfeiting purposes. This study demonstrates that the proposed surface engineering strategy provides an effective approach for producing clickable CNF and fabricating cellulosic materials with diverse functionalities that meet the demands of various applications.

1. Introduction

Cellulose, the most abundant biopolymer in nature, can be deconstructed into nanoscale fibrils known as cellulose nanofibrils (CNF) (Li et al., 2021; Moon, Martini, Nairn, Simonsen, & Youngblood, 2011). CNF exhibits remarkable features, including low density, high modulus, low thermal expansion coefficient, and so on (Li et al., 2024; Moon et al., 2011; Thomas et al., 2018). Bamboo, a fast-growing plant, is primarily composed of bamboo fibers (BF) and parenchyma cells (PC) in cell walls (Wang, Zhang, Jiang, Li, & Yu, 2015). Bamboo fibers are commonly used in various industries, such as papermaking, textiles, and composite materials (Liu, Song, Anderson, Chang, & Hua, 2012; Silva, Menis-Henrique, Felisberto, Goldbeck, & Clerici, 2020). However, parenchyma cells are often discarded as processing waste. Both constitutional components are rich in cellulose, with reports indicating that nanofibrils are easier to release from parenchyma cells compared to bamboo fibers. There is potential in utilizing parenchyma cells as starting materials for nanocellulose production (De France, Zeng, Wu, & Nyström, 2021;

Zhang et al., 2022). In this study, cellulose was extracted from parenchyma cells to be utilized as starting materials for CNF production and their subsequent surface functionalities, and cellulose was also extracted from bamboo fibers as a control for comparison.

Mechanical fibrillation alone is insufficient to produce fine CNF, requiring high energy input. Chemical pretreatment is often needed by introducing negatively charged groups or positively charged groups onto cellulose surfaces, giving rise to electrostatic repulsion forces between fibrils and thus facilitating their liberation during mechanical disintegration. As exemplified by TEMPO (2,2,6,6-tetramethylpiperidine-1-oxyl radical)-mediated oxidation approach, the hydroxyl group at position 6 in the anhydroglucose units (AGU) can be selectively oxidized and converted into carboxylate groups, thus adding negative charges onto the cellulose surface (De Nooy, Besemer, & Van Bekkum, 1995; Isogai, Hänninen, Fujisawa, & Saito, 2018). Another effective chemical pretreatment technique is dicarboxylic anhydride esterification. Likewise, negatively charged carboxylate is introduced to the cellulose surface, accelerating nanofibrillation (Beaumont et al., 2021;

* Corresponding author at: International Centre for Bamboo and Rattan, Beijing 100102, China.

E-mail address: zhongth@icbr.ac.cn (T. Zhong).

<https://doi.org/10.1016/j.carbpol.2024.122786>

Received 28 May 2024; Received in revised form 18 September 2024; Accepted 19 September 2024

Available online 22 September 2024

0144-8617/© 2024 Elsevier Ltd. All rights are reserved, including those for text and data mining, AI training, and similar technologies.

Zhang et al., 2023; Zhou et al., 2024). These methods often yield CNF with a large specific surface area and a surface rich in hydroxyl groups and hydrophilic groups, i.e., carboxylate groups ($-\text{COO}^-$).

The relatively monotonous surface traits of CNF often restrict their practical application scope. Surface functionalization of CNF is an effective strategy to address the simplicity of the surface traits of cellulose nanomaterials, intending to expand the range of applications. For example, Xiang et al. (2022) utilized CNC as raw material and treated it with tannic acid to create tannin-coated CNC; subsequently, the reactive phenolic hydroxyl groups and double bonds of tannic acid reacted with octadecylamine by Schiff-base and Michael-addition, resulting in hydrophobic nanocellulose suitable for hydrophobic coating application. It has been reported that cellulose was chemically modified with citric acid and subsequently processed into nanocellulose through homogenization. The resulting nanocellulose was then combined with fluorescent carbon dots to create fluorescently labeled nanocellulose (Wang, Du, Hsu, & Uyama, 2023).

Click chemistry is a modular reaction, allowing for rapid and precise synthesis of complex structures and functionalities by assembling small building blocks; moreover, click chemistry often undergoes under mild reaction conditions without generating by-products (Deng, Shavandi, Okoro, & Nie, 2021; Kolb, Finn, & Sharpless, 2001; Rostovtsev, Green, Fokin, & Sharpless, 2002). The thiol-ene reaction, one of the most common types of click reaction, involves a free radical addition reaction between a thiol and an alkene catalyzed by a photoinitiator (Griesbaum, 1970; Hoyle & Bowman, 2010). Before clicking functionalization of CNF, the introduction of clickable ene or thiol groups on the surface or chain end of CNF is often required. Under the aid of an initiator and UV irradiation, a variety of chemical compounds containing thiols or ene groups can be covalently attached to the surface of CNF through a thiol-ene click reaction, allowing for the creation of CNF with diverse surface properties and functionalities. For example, Wang et al. (2021) demonstrated that cellulose nanocrystals (CNCs), obtained through concentrated sulfuric acid hydrolysis, were reacted with undecylenoyl chloride through esterification. This process introduced an active ene group from undecylenoyl moieties onto the CNC surface, allowing for the covalent fixation of octadecanethiol to the surface of undecylenoyl-modified CNC through a thiol-ene click reaction. As a result, the resultant functionalized CNC exhibited enhanced hydrophobicity and phase change functionality. Jiang, Mietner, and Navarro (2023) reported that cellulose nanofibers obtained by mechanical delamination of wood pulp as raw material could be grafted with diethylene glycol ethyl acrylate and 3-trimethylsilylprop-2-yne propyl acrylate using a free radical polymerization reaction. This enabled further click reactions with various fluorescent dyes.

As mentioned above, click chemistry is a powerful tool for surface modification of CNF with diverse functionalities. However, most click-functionalization for CNF started with the preparation of CNF by conventional nanofibrillation methods, followed by the introduction of clickable groups on the surface of CNF, and finally the functionalization via a click reaction (Wang et al., 2021). This process is complicated and laborious, so simplifying the production process of clickable CNF and click-functionalized CNF is highly necessary.

It was reported that the most widely explored influence on reaction rate was linked to the selection of alkene in the thiol-ene click reaction, and early experiments indicated that the ring-strained (e.g., norbornenes) and electron-rich (e.g., vinyl ethers) alkenes reacted most rapidly, while electron-poor alkenes reacted more slowly (Hoyle, Lee, & Roper, 2004). It is well-known that carboxylate groups are the most common negatively charged groups introduced to the surface of cellulosic fibers to accelerate the release of nanofibrils in most CNF production cases. In this study, we hypothesize that the grafting of a compound bearing both negatively charged carboxylate groups and highly reactive clickable norbornene (NB) groups to cellulosic fibers can service dual purposes: one is to facilitate nanofibrillation due to electrostatic repulsion forces induced by anionic charges, yielding fine

cellulose nanofibrils, the other is to endow the resultant CNF simultaneously with clickable sites that enable further diverse surface functionalization via click reactions to produce various CNF with versatile functionalities.

Herein, we screened and proposed 5-norbornene-2,3-dicarboxylic anhydride (NBDCA) esterification in a dimethyl sulfoxide (DMSO)/potassium hydroxide (KOH)/H₂O system for direct surface modification of bamboo-sourced cellulose. The introduction of negatively charged groups and clickable groups could be achieved through a "one-pot" NBDCA esterification approach, rather than through a multi-stage clickable CNF preparation and modification process, with negatively charged carboxylate groups facilitating the liberation of nanofibrils during high-pressure homogenization and the norbornene group providing clickable sites for diverse functionalization of CNF. The characteristics of the resultant clickable CNF were investigated in terms of morphology, crystallinity, carboxylate content, and thermal stability. To demonstrate the viability of clickable CNF to be potential for various surface modifications to obtain versatile CNF with diverse functionalities, hexadecanethiol and 7-mercapto-4-methyl coumarin were used as thiol-containing compound paradigms to react with the developed clickable CNF via a thiol-ene click reaction, yielding CNF products with enhanced surface hydrophobicity and imparted fluorescent functionality, respectively.

2. Materials and methods

2.1. Materials

Six-year-old Moso bamboo (*Phyllostachys edulis*), harvested from Zhejiang Province, China, was processed into bamboo strips by Anji Jia Cai Bamboo Products Factory (Anji, China). Dimethyl sulfoxide (DMSO, analytical reagent, 99 %), potassium hydroxide (KOH, electronic grade, 99.999 %), 5-norbornene-2,3-dicarboxylic anhydride (NBDCA, 99 %), hexadecanethiol (99 %) and photoinitiator 651 (99 %) were purchased from Aladdin (Shanghai, China). 7-mercapto-4-methyl coumarin (97 %) was purchased from Sigma Aldrich (Shanghai, China). *N,N*-Dimethylformamide (DMF, analytical reagent, 99.5 %) was purchased from Macklin Reagent. Peroxyacetic acid (15–18 %) was purchased from LUTE Chemical Technology (Shandong, China). Deionized water was obtained from Water Purification System (MW-20E, Mei Cheng, China).

2.2. Bleaching and separation of parenchyma cells and fibers

The bamboo strips, cut into 3–5 cm in length, were treated with an 8 wt% peroxyacetic acid solution at 85 °C for 8 h, followed by thoroughly washing with deionized water. Subsequently, the bamboo strips underwent treatment with a 5 wt% KOH solution at 90 °C for 8 h, followed by washing with deionized water to neutralize. Finally, bleached bamboo strips were subjected to water flushing and sieving with various mesh sizes to separate parenchyma cells from fibers. Bleached parenchyma cells were obtained through sieving with a 200-mesh screen, while bleached fibers were obtained using a 30-mesh screen.

2.3. Preparation of PCNF and FCNF

PC or BF (2 g) was suspended in DMSO (40 mL) containing KOH (40 mg) and deionized water (6 mL) and then microwave (power: 900 W) heated for 60 s. Subsequently, NBDCA (NBDCA/AGU molar ratio = 8:1) dissolved in DMSO was added. The esterification took place at room temperature for 30 min and then was terminated by adding a large amount of hot water. The obtained products were washed with water by filtration to remove chemical residues. The purified esterified cellulosic materials were diluted to 0.5 wt%, with a pH of 9. Finally, the esterified cellulosic materials were sequentially mechanically disintegrated using a kitchen blender for 4 min and then passing a microfluidizer (M-110EH-30, Microfluidics, USA) 10 passes, yielding clickable CNF. The resultant

CNF was designated as PCNF or FCNF based on bamboo cellulose sources from PC and BF, respectively.

The carboxylate content of CNF was expressed as charge density (σ_{charge} , mmol/g CNF) and determined by conductivity titration reported by Zhou et al. (2024). The degree of substitution (DS) was determined following the method reported by Zhang et al. (2023) and calculated by the following Eq. (1):

$$DS = \frac{162 \times \sigma_{charge}}{10^3 - 186 \times \sigma_{charge}} \quad (1)$$

where 162 (g mol^{-1}) is the molecular mass of the anhydroglucose units in cellulose ($\text{C}_6\text{H}_{10}\text{O}_5$), and 186 (g mol^{-1}) is the molecular mass gain from $\text{C}_9\text{H}_7\text{O}_3\text{Na}$.

The yield of CNF was calculated following Eq. (2) reported by Zhou et al. (2024):

$$\text{yield} = \frac{(m_{\text{CNF}} - m_{\text{NBDCA}})}{m_c} \times 100\% \quad (2)$$

where m_{CNF} is the total mass of CNF, m_{NBDCA} is the mass of the grafted NBDCA, and m_c is the total mass of BF or PC used in the esterification reaction.

2.4. Hydrophobic modification

Hexadecanethiol (0.328 g) and photoinitiator 651 (4 mg) were added into the CNF (0.2 g) suspension in ethanol (10 mL). The mixture under stirring was exposed to 365 nm UV light with an intensity of 130 mW/cm^2 for 2 h at room temperature, hexadecanethiol modified CNF was washed with 70 °C ethanol by filtration to remove chemical residues. Based on the sources of CNF deriving from PC and BF, the obtained products were labeled as C16-PCNF or C16-FCNF, respectively.

2.5. Fluorescence labeling of CNF

7-Mercapto-4-methylcoumarin (32 mg), a sodium phosphate buffer solution (7 mL and $\text{pH} = 7$), and photoinitiator 651 (6 mg) were dissolved into DMSO (50 mL). CNF in DMSO was added, and the suspension was exposed to 356 nm UV light with an intensity of 130 mW/cm^2 for 2 h at room temperature under stirring. The fluorescence-labeled CNF was purified by centrifugation at 8000 rpm for 10 min for 4 cycles in fresh DMSO, and then thoroughly washed with deionized water by filtration. Based on the sources of CNF deriving from PC and BF, the obtained fluorescence-labeled CNF was designated as M-PCNF or M-FCNF, respectively.

2.6. Characterizations

The morphology of PC and BF after bleached and separation were analyzed by optical microscope (DMLB2, Laica, Germany) and scanning electron microscope (SEM, GeminiSEM360, Zeiss, Germany). The chemical compositions (glucan and xylan, and lignin) of PC and BF were determined according to NREL/TP-510-42618. The degree of polymerization (DP) was measured according to ASTM D1795-13. The crystallinity was performed using X-ray diffractometer (XRD, D8 advance, Bruker, Germany) operated with Cu K α radiation ($\lambda = 0.154$ nm). The crystallinity index (CrI) was calculated using the following Eq. (3) (Segal, Creely, Martin, & Conrad, 1959):

$$CrI = \frac{I_{200} - I_{am}}{I_{200}} \quad (3)$$

where I_{200} represents the diffraction intensity of the (200) crystalline plane, and I_{am} represents the diffraction intensity of the amorphous peak at $2\theta = 18.3^\circ$. The apparent crystallite size (ACS) was calculated using the Scherrer Eq. (4) (Popescu, Popescu, Lisa, & Sakata, 2011):

$$ACS = \frac{K \times \lambda}{\beta \times \cos\theta} \quad (4)$$

where K is constant 0.89, λ is the X-ray wavelength (0.154 nm), β is the half-height width of the diffraction band, and θ is the Bragg angle corresponding to the plane.

The morphology of the resultant CNF was observed using atomic force microscopy (AFM, Dimension ICON, Bruker, Germany) with tapping mode. The light transmittance of the resultant CNF suspensions was recorded with a UV-vis spectrophotometer (Lambda 35, PerkinElmer, USA) measuring at a wavelength of 400–800 nm. Fourier transform infrared spectroscopy (FTIR, Nexus 670, Thermo Fisher Scientific, USA) and the solid-state ^{13}C NMR spectrometry (Avance III, Bruker, Switzerland) were used to characterize the chemical structures of the bamboo cellulosic starting materials and the resultant CNF. NMR spectrometer was equipped with a 4 mm CPMAS probe. The spinning speed was 10 kHz, relaxation delay was 2 s and a typical number of 2000 scans were acquired for each spectrum. The thermal stability of bamboo cellulosic starting materials and the resultant CNF was carried out using a thermogravimetric (TG) analyzer (TGA4000, PerkinElmer, USA) under a nitrogen atmosphere with a flow rate of 20 mL/min, and with a temperature ramping up from 30 to 600 °C at 10 °C/min. Static water contact angles (WAC) were measured using a contact angle meter (OCA20, Dataphysics Instrument, Germany). Fluorescence spectra of M-FCNF and M-PCNF suspensions with different Fe^{3+} concentrations were obtained using a fluorescence spectrophotometer (F280, Gang Dong, China) at an excitation wavelength of 335 nm. Fluorescence images of M-PCNF and M-FCNF at an excitation wavelength of 405 nm were taken using intelligent laser scanning confocal microscopy (LSCM, Stellaris 5, Leica, Germany).

3. Results and discussion

3.1. Extraction of cellulosic materials from parenchyma cells and bamboo fibers

Fig. 1 depicts the fabrication process of bamboo-sourced clickable CNF via norbornene-dicarboxylic anhydride esterification followed by homogenization; subsequently, the resulting CNF with reactive clickable sites can undergo click modification for the generation of CNF with diverse surface functionality. First, bamboo cellulosic materials were extracted from PC and BF by a two-step bleaching process involving peracetic acid and potassium hydroxide. Cell walls swelled and softened during this process, and the non-cellulosic matrix, i.e., lignin, was removed. This led to the collapse of cell walls, making PC easier to separate from BF with the aid of water flushing and manual rubbing. Secondly, further sieving resulted in two types of bamboo cellulosic materials with distinct shapes. Fig. 2 shows morphology, chemical composition, DP, and cellulose crystallinity of these two bamboo cellulosic materials. As indicated by Fig. 2a–b, the developed separation process successfully yielded relatively pure PC and BF.

PC appeared in powder form, while BF exhibited a fibrous shape, as displayed in the respective Fig. 2a–b. The PC cavities appeared collapsed and wrinkled (Fig. 2c) after the bleaching and separation process, while BF almost remained unchanged in shape (Fig. 2d), although almost all lignin and partially hemicellulose were removed after bleaching process (Fig. 2e). Peracetic acid was effective in removing most of lignin, mainly because of the generation of hydroxyl radicals (HO^\bullet) and superoxide anion ($\text{O}_2^{\bullet-}$) radicals attacking the electron-rich aromatic rings and olefin side chain structures of lignin (Perez et al., 1998). Further alkali treatment eliminated the remaining lignin and partially removed hemicellulose, resulting in both PC and BF containing less than 0.5 % lignin (Fig. 2e). The DP of BF is slightly higher than that of PC (Fig. 2e). The diffraction patterns of the cellulosic materials exhibited characteristic peaks at $2\theta = 15^\circ$, corresponding to (1–10) and (110) crystalline planes,

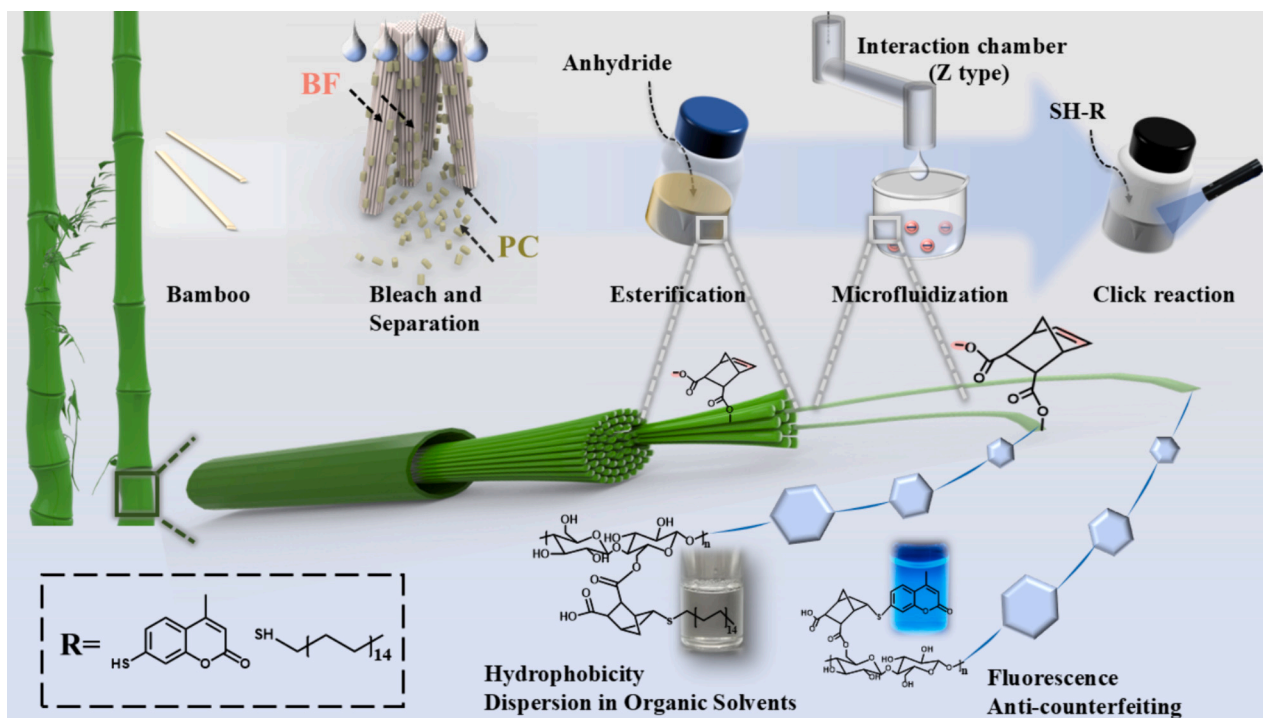


Fig. 1. Schematic diagram of the fabrication process of bamboo-sourced clickable CNF and their subsequent surface modifications through thiol-ene click reactions.

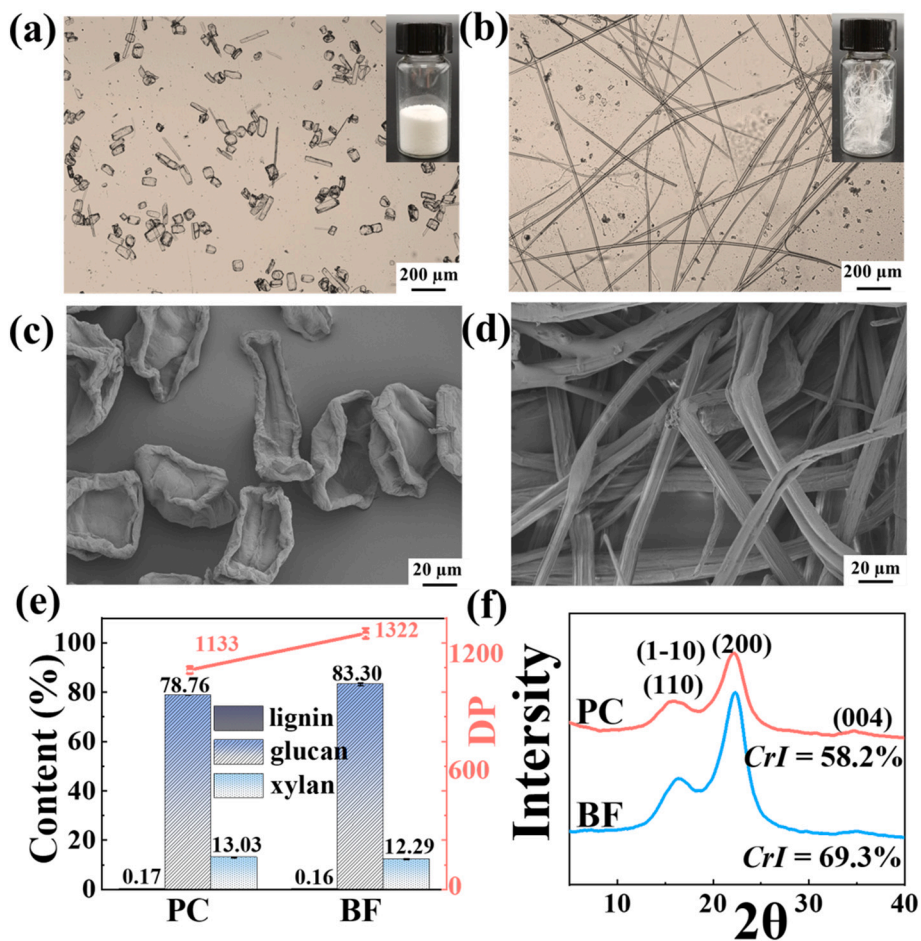


Fig. 2. Optical microscopic images of (a) bleached PC and (b) bleached BF (inset: corresponding digital photographs). SEM images of (c) bleached PC and (d) bleached BF; (e) chemical compositions and DP and (f) XRD patterns of bamboo cellululosic materials.

and at $2\theta = 22^\circ$ for (200) crystalline plane, indicating that both PC and BF are cellulose I, and the crystallinity of BF was higher than that of PC (Fig. 2f).

3.2. Morphology, crystallinity, and thermal stability of PCNF and FCNF

PC and BF first underwent swelling and activation in the DMSO/KOH/H₂O system under a 60-second microwave treatment. Rapid esterification occurred at room temperature upon the addition of NBDCA, subsequent deprotonation resulted in the generation of negatively charged surface from carboxylate groups (–COONa), giving rise to interfibrillar electrostatic repulsion, thereby accelerating their nanofibrillation during subsequent homogenization. Consequently, highly fibrillated bamboo-sourced CNF was successfully obtained from both PC and BF sources, respectively. The negatively charged surface was beneficial for the colloidal stability of CNF in water. The suspensions were stable and highly transparent, as evidenced by a high transmittance of both CNF suspensions exceeding 95 % (Fig. 3g–h).

One hundred nanofibrils were randomly selected from AFM micrographs to measure the height and length of the resultant CNF (Fig. 3a–f). Both types of CNF exhibited average heights were less than 3 nm, indicating that most individualized nanofibrils could be obtained. It can be clearly observed that FCNF was relatively longer with a higher aspect ratio and exhibited an intertwined network structure. On the contrary, PCNF was a little shorter in length. The variation in morphology of the resultant CNF derived from different cellulosic sources may stem from the inherent difference in original morphology and crystallinity between PC and BF. The higher crystallinity of BF, along with more regular arrangement of cellulose molecular chains in BF, made it more challenging to completely break down into nanofibrils, so the network structure FCNF was evident in Fig. 3d. It was well known that BF had only a small lumen and thick walls, while PC had much larger cavities with thin walls, allowing for more efficient contact with solvents and reactants and facilitating activation and esterification reactions (Zhang et al., 2022). PCNF exhibited a little higher degree of esterification, as evidenced by the carboxylate content and the calculated DS in Fig. 3i. The higher content of negatively charged carboxylates on the cellulose surface resulted in a higher interfibrillar electrostatic repulsion force, making nanofibrils easier to liberate from PC during the defibrillation process, resulting in relatively finer PCNF. The yields for PCNF and

FCNF were 70.3 % and 62.9 %, respectively.

We conducted an additional control experiment using the same pretreatment (microfluidization with 10 passes of unmodified PC and BF), which produced mechanically fibrillated PC-derived CNF and BF-derived CNF. These were labeled as PCNF* and FCNF*, respectively, as shown in Fig. S1. Although microfluidization alone of unmodified PC or BF can produce nanofibrillated cellulose, as evidenced in Fig. S1a, the resulting nanofibers are larger and more heterogeneous compared to those obtained with NBDCA pretreatment (Fig. 3a–d). In contrast to the stable and transparent CNF suspensions (Fig. 3g) achieved with NBDCA pretreatment of PC and BF followed by microfluidization treatment, the PCNF* and FCNF* suspensions exhibited slight opaqueness (Fig. S1b) and some phase separation in the FCNF* suspension after 0.5 h of storage. The UV–vis spectra (Fig. S1c) further confirmed that the light transmittance of CNF suspensions prepared without NBDCA pretreatment was significantly lower than those prepared with NBDCA pretreatment (Fig. 3h). These results demonstrate that the introduction of carboxylate groups through NBDCA pretreatment facilitates nanofibrillation, producing smaller, more individualized, and uniform CNF.

As shown in Fig. 4a, PCNF and FCNF exhibited a significant change in the diffractograms compared to their respective PC and BF starting materials (Fig. 2f), while still retaining their characteristic peaks at $2\theta = 15^\circ$ and 22° . The crystallinity of both PCNF and FCNF exhibited a noticeable decrease, this might be likely due to the grafting of bulky NBDCA groups onto the CNF, disrupting the originally ordered arrangement of cellulose chains and decreasing cellulose crystallinity (Zhang, Li, Li, Gibril, & Yu, 2014). As shown in Fig. 4b compared to raw materials, the calculated crystallite size that PCNF and FCNF were found to be smaller than PC and BF, respectively. Fig. 4c–e shows typical TG and DTG curves of the resulting CNF compared to their respective starting materials. The thermal stability of CNF was lower than that of raw materials likely due to the introduction of carboxylate groups and decreased crystallinity. Both the onset degradation temperature and the temperature at the maximum degradation rate of PCNF and FCNF notably shifted to lower temperatures. For example, the onset degradation temperature and the maximum degradation temperature of FCNF decreased to 258°C and 310°C , respectively, compared to 344°C and 365°C for BF. PC and BF have similar thermal stability before and after being converted into CNF. It is interesting to note that CNF had more char residues than PC/BF, which might be largely due to the generation

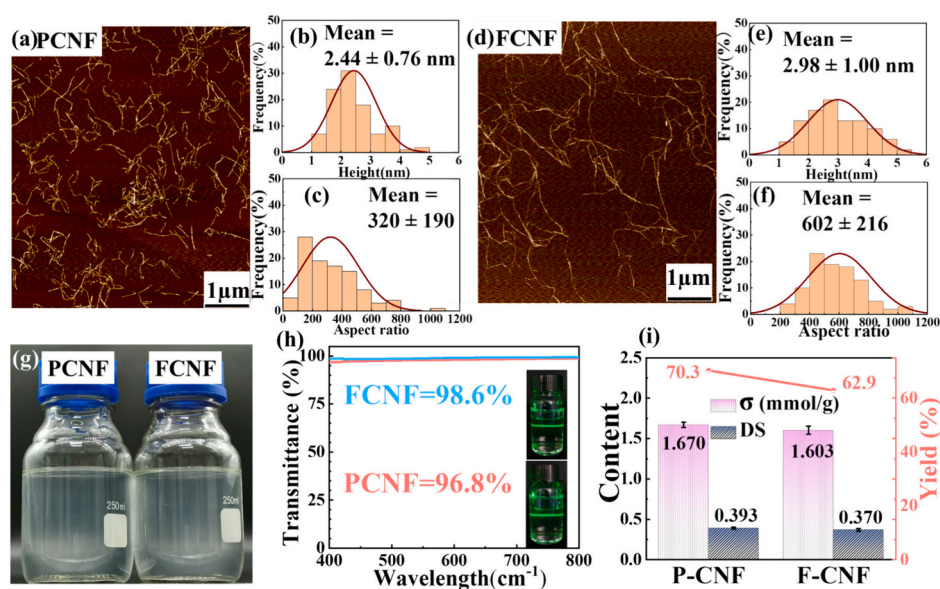


Fig. 3. AFM images (a) of the PCNF and the histograms of the corresponding size distribution (b) and aspect ratio (c). AFM images (d) of the FCNF and the histograms of the corresponding size distribution (e) and aspect ratio (f). Photographs (g) of PCNF and FCNF. Transmittance curves (h) of 0.1 wt% PCNFs and FCNFs under UV–vis (Inset: photographs of clear suspensions with green laser light passing through). (i) The carboxylate content, DS, and the yield of PCNF and FCNF.

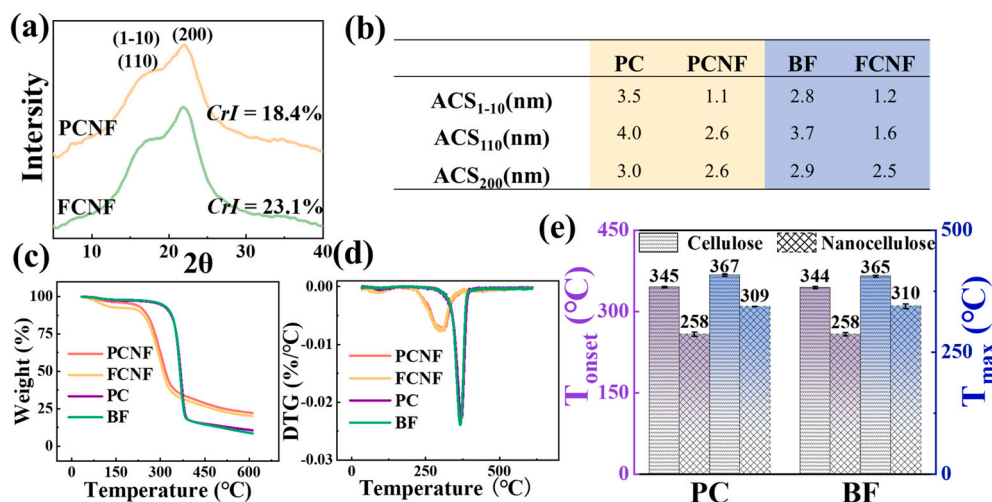


Fig. 4. (a) XRD curves of the resulting FCNF and PCNF. (b) Table presenting ACS values in raw materials and the resultant CNF. (c) TG curves, (d) DTG curves and (e) T_{onset} and T_{max} histograms of bleached PC, bleached BF and their resulting CNF.

of acid as a catalyst to promote the dehydration of cellulose during the pyrolysis of CNF bearing carboxylate groups, thus increasing char residues (Aoki & Nishio, 2010).

The FTIR spectra confirmed the successful grafting of the norbornene-dicarboxylic group onto the cellulose surface (Fig. 5a), as evidenced by the characteristic peaks of dicarboxylic acid groups at 1720 cm^{-1} and 1582 cm^{-1} , corresponding to the stretching vibrations of —COO— and —COONa , respectively. In addition, weak signals observed at 3090 cm^{-1} and 1687 cm^{-1} were assigned to the stretching vibrations of CH=CH_2 and C=C , respectively. After esterification modification, the characteristic peaks of the carbons of carboxylic acid groups were evident in the ^{13}C NMR spectrum (Fig. 5b), and the peaks at 175 ppm and 179 ppm were attributed to the carbons (C7, C10) from carbonyl ester groups in the open ring after the ring-opening esterification reaction, and the peaks at around 135 ppm corresponded to the carbons (C14, C15) from double bond in norbornene moiety, further confirming the successful grafting of norbornene-dicarboxylic group to cellulose.

3.3. Surface modification based on click reaction

In the thiol-ene click reactions, the reaction rate is largely determined by alkene structures, with cyclic norbornene known to exhibit greater reactivity due to the relief of ring strain upon the addition of double bonds to thiol radicals (Fairbanks et al., 2021; Hoyle et al., 2004). Therefore, norbornene dicarboxylic anhydride was chosen in this study to modify bamboo cellulose, serving dual purposes. First, it introduced negatively charged carboxylate groups to facilitate the liberation of nanofibrils during the subsequent mechanical disintegration stage. Second, it imparted cellulose surface with norbornene moieties containing highly reactive ene groups, thereby providing reactive clickable sites that enabled further functionalization of CNF via thiol-ene click reactions (Fig. 5c).

Hexadecanethiol was chosen for the surface modification of CNF bearing NB moieties, the thiol groups in hexadecanethiol were able to click with the ene groups in NB attached to CNF. This was confirmed by the FTIR analysis (Fig. 5a). The disappearance of characteristic peaks at 3090 cm^{-1} and 1687 cm^{-1} in its FTIR spectra indicated the removal of the double bond in NB groups upon click reaction. Conversely, the appearance of a symmetric peak at 2850 cm^{-1} and asymmetric peak at 2920 cm^{-1} of the methylene group from hexadecanethiol suggested the successful grafting of a long aliphatic chain onto the CNF surface through a thiol-ene click reaction. The ^{13}C NMR results further confirmed the successful grafting of hexadecanethiol to CNF via thiol-ene click reaction, as evidenced by the disappearance of the characteristic

peak at 135 ppm associated with carbons from carbon-carbon double bonds. An interesting observation is the shift of the characteristic peak of C10 at 179 ppm in the ^{13}C NMR spectra of the resultant CNF towards the right, overlapping with the peak of C7 at 175 ppm to form a characteristic peak (Fig. 5b). This shift might be largely attributed to the protonation of CNF before hydrophobic modification, where the —COONa on the surface was converted into —COOH .

7-mercapto-4-methylcoumarin contains an active thiol group while possessing fluorescence functionality, allowing it to react with NB-containing CNF via a thiol-ene click reaction, thereby imparting fluorescence functionality to CNF. The peaks at 1645 cm^{-1} and 1510 cm^{-1} corresponding to the stretching vibration of the benzene ring skeleton C=C in 7-mercapto-4-methylcoumarin, along with the peak at 1373 cm^{-1} corresponding to the bending vibration of CH_3 , were observed in the FTIR spectra after fluorescence labeling (Fig. 5a). Additionally, the ^{13}C NMR spectra of the fluorescence-labeled CNF demonstrated the presence of the characteristic peak of carbon (C34) from methyl group was evident at 40 ppm (Fig. 5b), providing further evidence of the successful grafting of 7-mercapto-4-methyl coumarin onto the surface of CNF.

The carboxylated CNF surface was rich in hydroxyl groups and carboxylate group (—COO^-), imparting strong hydrophilicity and allowing for stable dispersion in water, making it favorable for applications in aqueous systems like water-based paints and hydrogels. However, the hydrophilic nature of hydroxyl groups on the surface of cellulose hindered their dispersibility in organic solvents and hydrophobic environments, limiting their application in organic solvents or non-aqueous environments. A common method of surface hydrophobic modification is to introduce a long aliphatic chain onto the CNF surface. As previous discussion above, CNF with clickable groups was successfully produced, enabling the grafting of long aliphatic chains onto CNF for hydrophobic modification via click reaction. The surface of the different films made from CNF before and after hydrophobization was relatively smooth, as seen in Fig. S2. The water contact angle (WCA) of thin films made from CNF and dried C16-CNF was tested, revealing an increase in WCA of C16-FCNF from 58° to 101° (Fig. 6a). Elemental analysis for the samples after click reaction was performed, and the result is presented in Table S1. The weight percentage of a sulfur element in the CNF after thiol-ene reaction was a little higher in the BF-sourced CNF, suggesting that more grafting of thiol-containing compounds occurred. That might largely explain why the WCA for the C16-FCNF derived from BF was a little higher, because more thiol-containing compounds with hydrophobic long aliphatic chains were introduced to the CNF surface. To assess the dispersibility of the hydrophobically

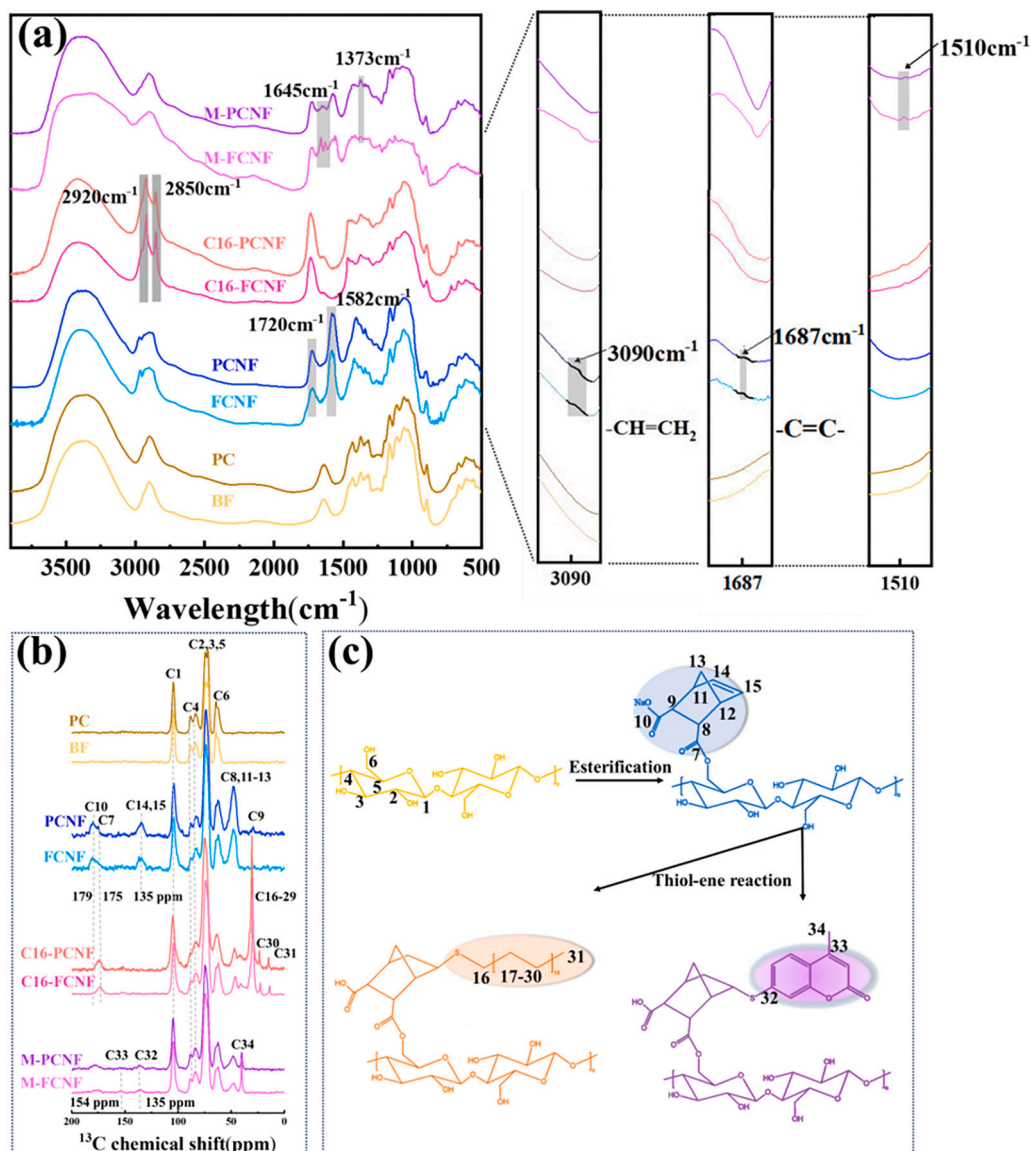


Fig. 5. (a) FTIR spectra of PC, BF, PCNF, FCNF, C16-PCNF, C16-FCNF, M-PCNF and M-FCNF, in which the 3400–2900 cm⁻¹ region, 1730–1650 cm⁻¹ and 1530–1480 cm⁻¹ region were amplified; (b) solid-state ¹³C NMR; (c) reaction process.

modified CNF in different solvents, three commonly used solvents (DMSO, DMF, and water) were used in this study (Fig. 6b). Before modification, the dispersion of CNF in DMSO and DMF was relatively poor, as evidenced in Fig. S3. The hydrophobically modified CNF exhibited good dispersion in DMSO and DMF, making it potential to be used in the applications where organic systems are required. The combination of the hydrophobic nature of surface-functionalized CNF and the polar characteristics of DMSO and DMF with high dielectric constant and strong solvation likely contributed to the improvement in its dispersibility in this solvent. This further confirmed that the hydrophobic modification of CNF with improved dispersibility in common solvents such as DMSO and DMF could be achieved through click reaction with hexadecylthiol.

Coumarin is a natural compound with weak fluorescence. Its derivative, 7-mercapto-4-methyl coumarin, is water-insoluble and exhibits almost no fluorescence in water (Lanterna, González-Béjar, Frenette, & Scaiano, 2017). However, when 7-mercapto-4-methyl coumarin was linked with NB attached to CNF through a thiol-ene click reaction, it endowed CNF with fluorescence functionality. The increased fluorescence may be due to the thiol-alkylation of 7-mercapto-4-

methylcoumarin (Lanterna et al., 2017), where the alkyl chain may act as a medium for energy transfer, helping to transfer the excitation energy from the core region of the fluorophore to the luminescent center, reducing energy loss. As a result, the fluorescence signal is amplified, enabling CNF to exhibit fluorescence functionality (Fan, Hu, Zhan, & Peng, 2013). Furthermore, the covalent attachment of coumarin derivative to the CNF surface via a thiol-ene click reaction could help prevent aggregation of fluorescent molecules, thereby enhancing their stability. This not only helped to mitigate the aggregation-induced quenching (ACQ) effect but also enhanced the fluorescence properties of CNF (Nawaz et al., 2022; Tian et al., 2016). In UV-vis spectroscopy, both M-PCNF and M-FCNF exhibited absorption peaks at 272 nm and 340 nm (Fig. 6c). The 272 nm absorption peak arose from mainly caused by $\pi \rightarrow \pi^*$ transitions of C=C bonds, and the 340 nm absorption peak was mainly due to $n \rightarrow \pi^*$ transitions of C=O bonds (Wang et al., 2023). As seen from fluorescence spectra, the maximum intensity was observed at 448 nm when excited at 335 nm (Fig. 6d).

Additionally, fluorescence-labeled M-CNF was found to retain the essential features of CNF, including favorable dispersibility in aqueous solutions, excellent film-forming attributes, and high transparency and

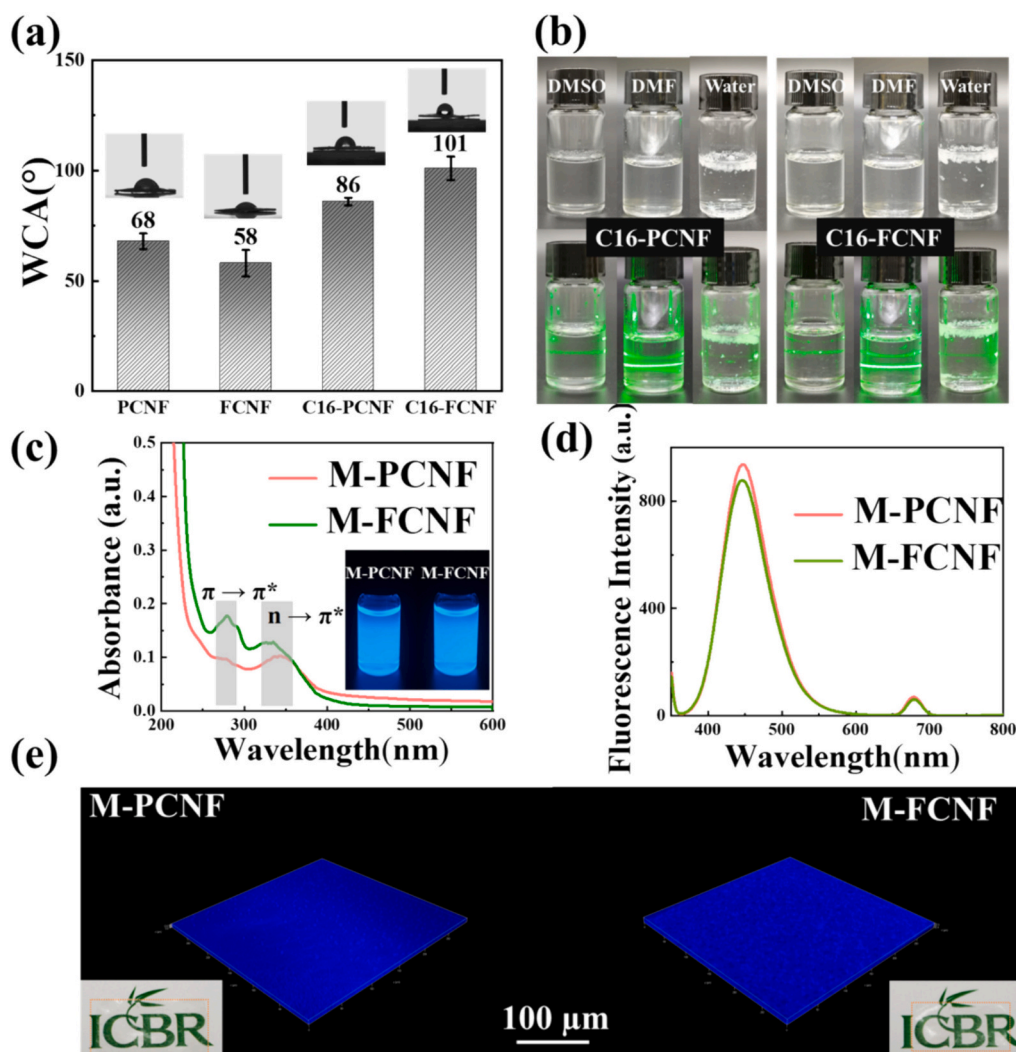


Fig. 6. (a) Water contact angles; (b) photographs showing the dispersion of C16-PCNF and C16-FCNF in solvents. The super colloidal stability in organic solvents is indicated by the Tyndall effect; (c) UV-vis spectra of M-PCNF and M-FCNF (inset: photographs of M-PCNF and M-FCNF suspensions under 365-nm UV light) and (d) fluorescence measurements of 0.1 wt% M-PCNF and M-FCNF; (e) laser scanning confocal microscopy imaging of films of M-PCNF and M-FCNF (inset: corresponding digital photographs of CNF films).

flexibility of the ensuing films. Both aqueous solutions and films of M-PCNF and M-FCNF exhibited fluorescence behavior under 365 nm UV light, emitting blue light (Fig. 6c). Fluorescent film imaging can be observed by LSCM, with fluorescence essentially covering the entire film surface (Fig. 6e). CNF can provide an ideal environment for the covalent fixation of coumarin derivative to its surface, allowing for efficient distribution of fluorescence molecules and prevention of aggregation, thereby inducing good fluorescence properties. Meanwhile, CNF has excellent film-forming capability, yielding the ensuing nano-fluorescent flexible films with fluorescence properties.

The stable fluorescence performance of M-CNf can be used for detecting Fe^{3+} ions in water. The fluorescence intensities of M-PCNF and M-FCNF both gradually decrease with the increase in Fe^{3+} ion concentration (from 1 mg/L to 100 mg/L) (Fig. 7a–f). This was likely attributed to the characteristic ability of 7-mercaptoyl-4-methyl coumarin to accept transition metals and form metal chelates (El-Sawy, Abdelwahab, & Kirsch, 2022). Additionally, as the Fe^{3+} concentration increased, the fluorescence gradually quenched under UV light (365 nm) irradiation, while the color changes from colorless to yellow in visible light (Fig. 7a, d). Remarkably, linear relationships between the fluorescence intensity (F_0/F) of M-PCNF and M-FCNF and the concentration of Fe^{3+} ions were established. F_0 and F represent the fluorescence intensities of the M-CNf

suspension before and after the addition of the metal ion solution, respectively. As discussed above, more thiol-containing compound was introduced to FCNF through thio-ene click reaction, so M-FCNF had higher coumarin content. The lower limit of detection of Fe^{3+} for M-FCNF and M-PCNF was also closely related to grafted coumarin. The detection limits for Fe^{3+} ions of M-PCNF and M-FCNF were 0.39 mg/L and 0.68 mg/L, respectively, determined by the formula $3\delta/S$ reported by Nawaz et al. (2022), where δ is the standard deviation of the lowest signal and S is the slope of the linear graph (Nawaz et al., 2022). The fluorescence-labeling CNF can potentially be used in anti-counterfeiting marks on identity cards, currency, and commodities, as well as for anti-counterfeiting inks used in information encryption applications. Fig. 7h demonstrates the use of M-CNf suspension for covert writing marks with a brush pen and a ballpoint pen.

We have compared our work with other reported studies in the literature regarding the thiol-ene reaction in nanocellulose, as presented in Table S2. Comparing the thiol-ene reaction efficiency of CNF grafted with norbornene moieties to other studies in the literature is challenging due to differences in nanocellulose types, thiols and ene, reaction conditions, and light intensities used. As previously mentioned, cyclic norbornene exhibits high reactivity due to the relief of ring strain when thiol radicals undergo a reaction with double bonds in the cyclic

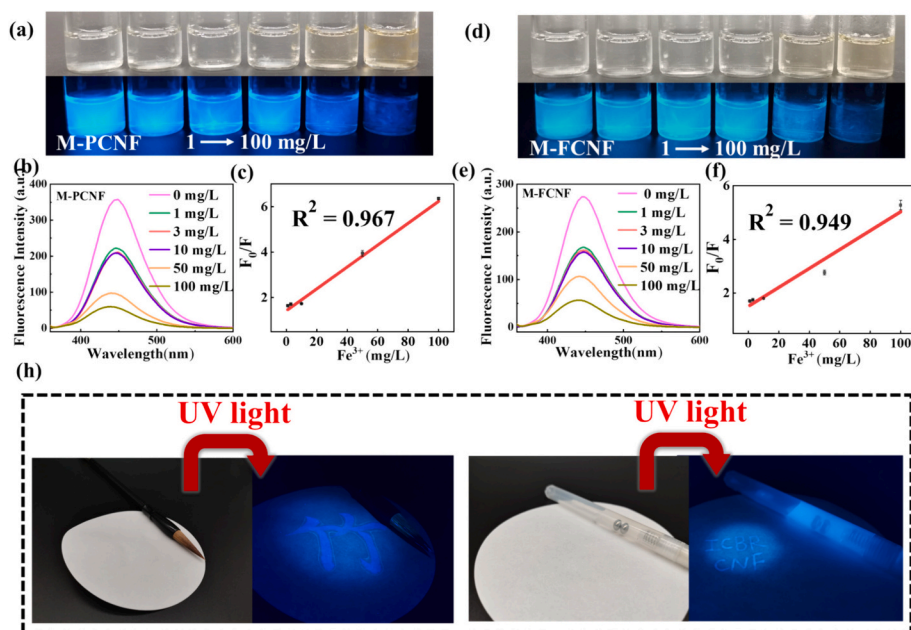


Fig. 7. Photographs of (a) M-PCNF and (d) M-FCNF suspensions (2 mL, 0.1 wt%) by adding different concentrations of 2 mL Fe^{3+} ions aqueous solutions (1 to 100 mg/L) under sunlight (top) and 365 nm UV light (bottom). Fluorescence spectra of (b) M-PCNF and (e) M-FCNF and (c, f) their respective graphs displaying the linear relationship between the concentration of Fe^{3+} ions and fluorescence intensity. (g) Photographs of paper with writing with fluorescence-labeled CNF used as ink observed under sunlight and UV light.

norborene (Fairbanks et al., 2021; Hoyle et al., 2004). In this study, it is encouraging to note that that thiol-ene reaction of CNF grafted with norbornene moieties occurred within a relatively short time as shown in Table S2, imparting diverse functionalities to the CNF.

4. Conclusions

In this study, we have proven a successful grafting a compound with both negatively charged carboxylate groups and highly reactive clickable NB groups to the surface of bamboo-sourced cellulose via 5-norbornene-2,3-dicarboxylic anhydride (NBDCA) esterification, which not only has facilitated the liberation of nanofibrils, but also has provided CNF with clickable capability simultaneously.

With the aid of electrostatic repulsion forces generated by negatively charged carboxylate groups, fine CNF with a small diameter of around 3 nm, a high aspect ratio of up to 600, and a high surface charge (around 1.6 mmol/g CNF), and bearing highly reactive clickable norbornene groups, were successfully obtained from both bamboo-sourced cellulosic materials. Furthermore, we have also demonstrated that the NB groups attached to the surface of the resultant CNF could react with various thiol-containing compounds through a thiol-ene click reaction. Hexadecanethiol could successfully click with the NB-containing CNF, imparting CNF with enhanced hydrophobicity and well dispersion ability in organic solvents such as DMSO and DMF. 7-mercapto-4-methyl coumarin, a thiol-containing compound, also could click with this NB-containing CNF, endowing it with fluorescent functionality and Fe^{3+} detection capability.

To our knowledge, the direct grafting of a compound with both carboxylate groups and NB groups to cellulosic fibers via the NBDCA esterification for the manufacturing of clickable CNF was reported for the first time. This surface engineering strategy proved facile and effective in producing a clickable CNF. Diverse functionalities of CNF can be further designed and achieved based on click reactions. For example, but not limited, the developed hydrophobic modified CNF could be expanded to be utilized in organic solvent systems and the fluorescence-labeling CNF with good aqueous dispersibility can be utilized as smart inks for anti-counterfeiting applications or

environmentally friendly sensors for Fe^{3+} detection. The clickable sites on the surface of the developed CNF offer many potential possibilities for further surface modification with the expectation of yielding versatile CNF products to meet various demands for diverse applications.

CRediT authorship contribution statement

Juan Long: Writing – original draft, Methodology, Investigation, Data curation. **Zhiqiang Li:** Writing – review & editing, Methodology, Conceptualization. **Tuhua Zhong:** Writing – review & editing, Project administration, Methodology, Funding acquisition, Conceptualization.

Declaration of competing interest

The authors declare that they have no known competing financial interests or personal relationships that could have appeared to influence the work reported in this paper.

Data availability

Data will be made available on request.

Acknowledgments

This work was supported by the Fundamental Research Funds of the International Centre for Bamboo and Rattan (ICBR) (1632023017) and the National Key Research & Development Program of China (2022YFD2200901).

Appendix A. Supplementary data

Supplementary data to this article can be found online at <https://doi.org/10.1016/j.carbpol.2024.122786>.

References

- Aoki, D., & Nishio, Y. (2010). Phosphorylated cellulose propionate derivatives as thermoplastic flame resistant/retardant materials: Influence of regioselective phosphorylation on their thermal degradation behaviour. *Cellulose*, *17*(5), 963–976.
- Beaumont, M., Tardy, B. L., Reyes, G., Koso, T. V., Schaubmayr, E., Jusner, P., ... Rosenau, T. (2021). Assembling native elementary cellulose nanofibrils via a reversible and regioselective surface functionalization. *Journal of the American Chemical Society*, *143*(41), 17040–17046.
- De France, K., Zeng, Z., Wu, T., & Nyström, G. (2021). Functional materials from nanocellulose: utilizing structure–property relationships in bottom-up fabrication. *Advanced Materials*, *33*(28), Article 2000657.
- De Nooy, A. E. J., Besemer, A. C., & Van Bekkum, H. (1995). Highly selective nitroxyl radical-mediated oxidation of primary alcohol groups in water-soluble glucans. *Carbohydrate Research*, *269*(1), 89–98.
- Deng, Y., Shavandi, A., Okoro, O. V., & Nie, L. (2021). Alginate modification via click chemistry for biomedical applications. *Carbohydrate Polymers*, *270*, Article 118360.
- El-Sawy, E. R., Abdelwahab, A. B., & Kirsch, G. (2022). Insight on mercapto-coumarins: Synthesis and reactivity. *Molecules*, *27*(7), Article 7.
- Fairbanks, B. D., Macdougall, L. J., Mavila, S., Sinha, J., Kirkpatrick, B. E., Anseth, K. S., & Bowman, C. N. (2021). Photoclick chemistry: A bright idea. *Chemical Reviews*, *121*(12), 6915–6990.
- Fan, J., Hu, M., Zhan, P., & Peng, X. (2013). Energy transfer cassettes based on organic fluorophores: Construction and applications in ratiometric sensing. *Chemical Society Reviews*, *42*(1), 29–43.
- Griesbaum, K. (1970). Probleme und Möglichkeiten der radikalischen Addition von Thiolen an ungesättigte Verbindungen. *Angewandte Chemie*, *82*(7), 276–290.
- Hoyle, C. E., & Bowman, C. N. (2010). Thiol-ene click chemistry. *Angewandte Chemie International Edition*, *49*(9), 1540–1573.
- Hoyle, C. E., Lee, T. Y., & Roper, T. (2004). Thiol–enes: Chemistry of the past with promise for the future. *Journal of Polymer Science Part A: Polymer Chemistry*, *42*(21), 5301–5338.
- Isogai, A., Hänninen, T., Fujisawa, S., & Saito, T. (2018). Review: Catalytic oxidation of cellulose with nitroxyl radicals under aqueous conditions. *Progress in Polymer Science*, *86*, 122–148.
- Jiang, X., Mietner, J. B., & Navarro, J. R. G. (2023). A combination of surface-initiated controlled radical polymerization (SET-LRP) and click-chemistry for the chemical modification and fluorescent labeling of cellulose nanofibrils: STED super-resolution imaging of a single fibril and a single fibril embedded in a composite. *Cellulose*, *30*(5), 2929–2950.
- Kolb, H. C., Finn, M. G., & Sharpless, K. B. (2001). Click chemistry: Diverse chemical function from a few good reactions. *Angewandte Chemie International Edition*, *40*(11), 2004–2021.
- Lanterna, A. E., González-Béjar, M., Frenette, M., & Scaiano, J. C. (2017). Photophysics of 7-mercapto-4-methylcoumarin and derivatives: Complementary fluorescence behaviour to 7-hydroxycoumarins. *Photochemical & Photobiological Sciences*, *16*(8), 1284–1289.
- Li, T., Chen, C., Brozena, A. H., Zhu, J. Y., Xu, L., Driemeier, C., ... Hu, L. (2021). Developing fibrillated cellulose as a sustainable technological material. *Nature*, *590*(7844), 47–56.
- Li, Y., Jiao, H., Zhang, H., Wang, X., Fu, Y., Wang, Q., Liu, H., Yong, Y., Guo, J., & Liu, J. (2024). Biosafety consideration of nanocellulose in biomedical applications: A review. *International Journal of Biological Macromolecules*, *265*, Article 130900.
- Liu, D., Song, J., Anderson, D. P., Chang, P. R., & Hua, Y. (2012). Bamboo fiber and its reinforced composites: Structure and properties. *Cellulose*, *19*(5), 1449–1480.
- Moon, R. J., Martini, A., Nairn, J., Simonsen, J., & Youngblood, J. (2011). Cellulose nanomaterials review: Structure, properties and nanocomposites. *Chemical Society Reviews*, *40*(7), 3941.
- Nawaz, H., Chen, S., Li, X., Zhang, X., Zhang, X., Wang, J.-Q., & Xu, F. (2022). Cellulose-based environment-friendly smart materials for colorimetric and fluorescent detection of Cu²⁺/Fe³⁺ ions and their anti-counterfeiting applications. *Chemical Engineering Journal*, *438*, Article 135595.
- Perez, D. D. S., Terrones, M. G. H., Grelier, S., Nourmamode, A., Castellan, A., Ruggiero, R., & Machado, A. E. H. (1998). Peroxyformic acid pulping of eucalyptus grandis wood chips and sugar cane bagasse in one stage and characterization of the isolated lignins. *Journal of Wood Chemistry and Technology*, *18*(3), 333–365.
- Popescu, M.-C., Popescu, C.-M., Lisa, G., & Sakata, Y. (2011). Evaluation of morphological and chemical aspects of different wood species by spectroscopy and thermal methods. *Journal of Molecular Structure*, *988*(1–3), 65–72.
- Rostovtsev, V. V., Green, L. G., Fokin, V. V., & Sharpless, K. B. (2002). A stepwise Huisgen cycloaddition process: copper(I)-catalyzed regioselective “ligation” of azides and terminal alkynes. *Angewandte Chemie International Edition*, *41*(14), 2596–2599.
- Segal, L., Creely, J. J., Martin, A. E., & Conrad, C. M. (1959). An empirical method for estimating the degree of crystallinity of native cellulose using the X-ray diffractometer. *Textile Research Journal*, *29*(10), 786–794.
- Silva, M. F., Menis-Henrique, M. E., Felisberto, M. H., Goldbeck, R., & Clerici, M. T. (2020). Bamboo as an eco-friendly material for food and biotechnology industries. *Current Opinion in Food Science*, *33*, 124–130.
- Thomas, B., Raj, M. C., B. A. K., H. R. M., Joy, J., Moores, A., ... Sanchez, C. (2018). Nanocellulose, a versatile green platform: From biosources to materials and their applications. *Chemical Reviews*, *118*(24), 11575–11625.
- Tian, W., Zhang, J., Yu, J., Wu, J., Nawaz, H., Zhang, J., ... Wang, F. (2016). Cellulose-based solid fluorescent materials. *Advanced Optical Materials*, *4*(12), 2044–2050.
- Wang, H., Zhang, X., Jiang, Z., Li, W., & Yu, Y. (2015). A comparison study on the preparation of nanocellulose fibrils from fibers and parenchymal cells in bamboo (*Phyllostachys pubescens*). *Industrial Crops and Products*, *71*, 80–88.
- Wang, J., Du, P., Hsu, Y.-I., & Uyama, H. (2023). Cellulose luminescent hydrogels loaded with stable carbon dots for duplicable information encryption and anti-counterfeiting. *ACS Sustainable Chemistry & Engineering*, *11*(27), 10061–10073.
- Wang, Y., Qiu, Z., Lang, Z., Xie, Y., Xiao, Z., Wang, H., ... Zhang, K. (2021). Multifunctional reversible self-assembled structures of cellulose-derived phase-change nanocrystals. *Advanced Materials*, *33*(3), 2005263.
- Xiang, H., Wang, B., Zhong, M., Liu, W., Yu, D., Wang, Y., ... Zhang, Z. (2022). Sustainable and versatile superhydrophobic cellulose nanocrystals. *ACS Sustainable Chemistry & Engineering*, *10*(18), 5939–5948.
- Zhang, D., Jin, K., Lim, K. H., Jie, S., Wang, W.-J., & Yang, X. (2023). Eco-friendly cellulose nanofibrils with high surface charge and aspect ratio for nanopaper films with ultrahigh toughness and folding endurance. *Green Chemistry*, 4696–4704.
- Zhang, X., Guo, F., Yu, Z., Cao, M., Wang, H., Yang, R., ... Salmén, L. (2022). Why do bamboo parenchyma cells show higher nanofibrillation efficiency than fibers: An investigation on their hierarchical cell wall structure. *Biomacromolecules*, *23*(10), 4053–4062.
- Zhang, Y., Li, H., Li, X., Gibril, M. E., & Yu, M. (2014). Chemical modification of cellulose by in situ reactive extrusion in ionic liquid. *Carbohydrate Polymers*, *99*, 126–131.
- Zhou, M., Chen, D., Chen, Q., Chen, P., Song, G., & Chang, C. (2024). Reversible surface engineering of cellulose elementary fibrils: From ultralong nanocelluloses to advanced cellulosic materials. *Advanced Materials*, *36*(21), Article 2312220.